Title

Optional subtitle

J. Random Author

Cover Text
possibly
spanning multiple lines

ISBN 000-00-0000-000-0

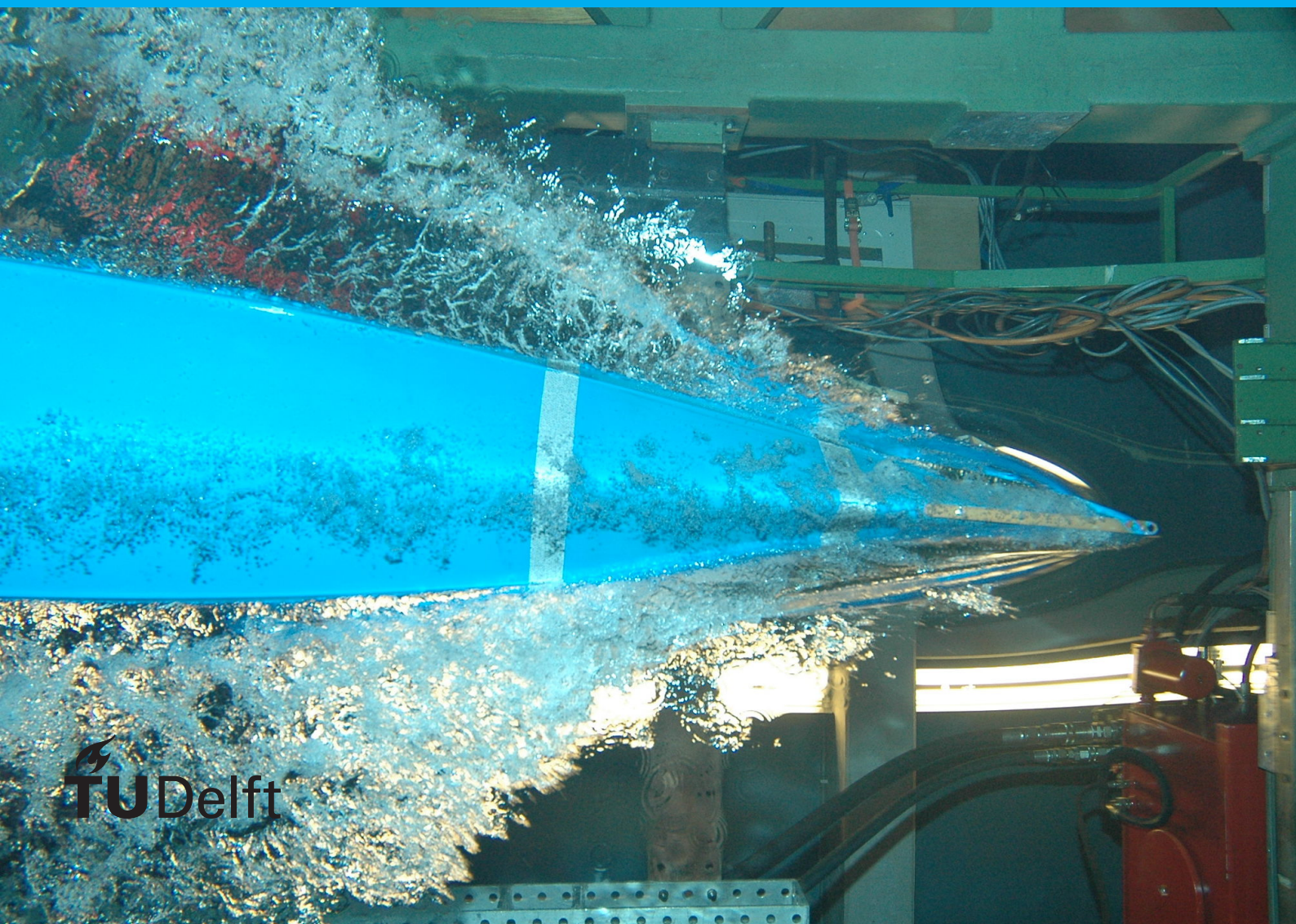

Title

Optional subtitle

by

J. Random Author

to obtain the degree of Master of Science
at the Delft University of Technology,
to be defended publicly on Tuesday January 1, 2013 at 10:00 AM.

Student number:	1234567	
Project duration:	March 1, 2012 – January 1, 2013	
Thesis committee:	Prof. dr. ir. J. Doe,	TU Delft, supervisor
	Dr. E. L. Brown,	TU Delft
	Ir. A. Aaronson,	Acme Corporation

This thesis is confidential and cannot be made public until December 31, 2013.

TU Delft

Preface

Preface…

J. Random Author
Delft, January 2013

Contents

1

Introduction

66 Million years ago, an asteroid the size of Rotterdam initiated what is perhaps the most well known cataclysmic event in the history of life on Earth. With an impact releasing the energy of a billion nuclear bombs, the asteroid left a 180 km crater in the Gulf of Mexico. Launching enough debris into the atmosphere to block out the light of the Sun, eventually leading to the extinction of three quarters of spiecies on Earth, most famously the non-avian dinosaurs (Chiarenza et al., 2020). In recorded human history, a multitude of noteworthy asteroids have impacted Earth, such as the Tunguska impactor in 1908 in Siberia. Flattening over 2000 km^2 of forest, events such as this serve as a staunch reminder of the massive kinetic energy that can be released by an object descending to Earth from space, and the danger this poses to human civilization.

Cognizant of such hazard, the United States launched the Spaceguard Survey in 1992, aiming to "identify 90% of near-Earth Asteroids (NEA's) larger than 1 km within 10 years." (Morrison, 1992). With improvements in observation technology, more meteors were witnessed and recorded, leading to greater awareness into the frequency and unpredictability of such events. Of course, impacts from space are not a problem exclusive to Earth; as the 1994 impact of comet Shoemaker-Levy 9 into Jupiter proved. This impact showed that impacts of objects large enough to cause global catastrophy were not as highly improbably as once considered, and asteroid identification efforts took off with it.

The initial spaceguard survey goal was completed succesfully, and it is known that there are - within reasonable probability - no civilization-ending asteroids destined for Earth impact in the coming millenium. Nevertheless, smaller asteroids can still pose a local threat to human life or property. In addition, much is still unknown about the exact population of near-Earth asteroids, and such knowledge might provide valuable insights into the origin and evolution of the Solar system. Therefore, NASA extended the spaceguard mandate to detect 90% of all NEA's larger than 140m (Harris, 2008).

Since then, a lot of progress has been made in cataloguing and identifying smaller NEA's. Additionally, consideration has been given to survey for smaller limiting diameters (e.g. Stokes et al., 2003). However, such efforts have to date still been very unsuccesful: For example, in 2013, a meteoric airburst over the city of Chelyabinsk, Russia, seriously injured almost 1500 people and damaged several thousands of buildings. Although damage was limited due to the high altitude of the explosion, no precautionary measures were taken, as the asteroid was completely unknown until the moment of atmospheric entry. Luckily, such events are not a common occurence. However, the large majority of NEA's of this size is completely unknown, and as such they can strike anywhere at any time.

1.1. Near-Earth Asteroids

Asteroids are perhaps the most diverse object in the Solar system: ranging in size from tiny chips to dwarf planets such as Vesta and Ceres; from rocky compositions, to fully metallic monoliths, and composites in various elements and mineral shapes; from close to the Sun on short orbits, to distant eccentric long period trajectories. All of this greatly increases the complexity of surveying for near-Earth

asteroid. Before continuing, the definition of a near-Earth asteroid will be given as follows: *a near-Earth asteroid is any asteroid with a perihelion* $q \leq 1.3\mathrm{AU}$ *and semi-major axis* $a \leq 4.2\mathrm{AU}$.

Current knowledge of the asteroid population is based on past and current NEA surveys. The most important parameter to consider is the size-frequency distribution of the objects. After all, larger objects exhibit a larger impact energy and hence threat, but small objects are more common and harder to detect. A good representation for this size-frequency distribution is a power law as follows:

$$\frac{dN}{dD_p} \propto D_p^{-k} \tag{1.1}$$

With exponent k in the range of 2.95 - 3.5 (Ivanov, 2008). Commonly, the size of the asteroid can not be directly ascertained; the target is too small to accurately determine the size. However, estimates can be made based on the absolute magnitude H of the object by relation with an assumed albedo p_v ($p_v = 0.14$ is often used as an approximation) using the relationship first derived by Bowell et al., 1989:

$$D = \frac{1329\mathrm{km}}{\sqrt{p_v}} \cdot 10^{-H/5} \tag{1.2}$$

As a result of the success of the spaceguard survey efforts, past efforts have more than likely identified all NEA's with $H \leq 15$, corresponsing to the *flying mountains* several kilometers in diameter. Also, at smaller limiting diameters, a lot of NEA's have been - and continue to be - found. The surveys through which this is achieved will be discussed in further detail in **??**. Through a process of modelling the asteroid population, and simulating the performance of past surveys on it, followed by fitting the results, Granvik et al., 2018 have produced a parametric model of the NEA population. The distribution of orbital elements in this model can be seen in Figure 1.1.

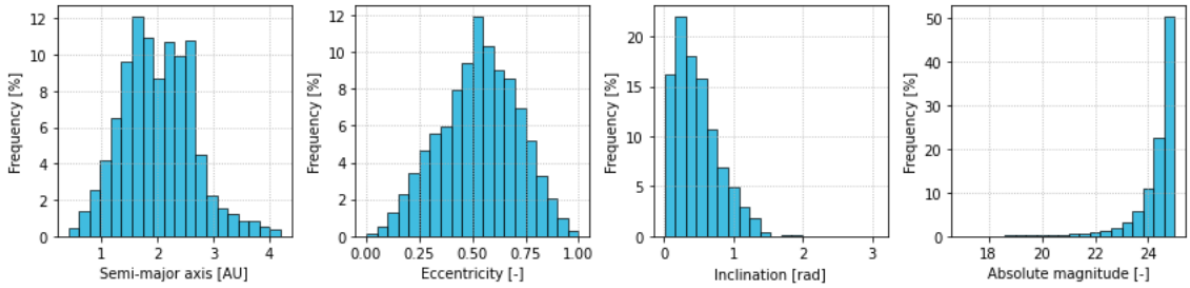

Figure 1.1: Frequency of orbital elements for modelled NEA population according to Granvik et al., 2018

.

Several things are of note: First and foremost, the population is very diverse; there is no particular concentration of NEA's anywhere that allows for simple exploitation in survey design. Secondly, the bulk of NEA's has a semi-major axis of $1.0\mathrm{AU} < a < 3.0\mathrm{AU}$. The dips at $a = 2.0\mathrm{AU}$ and $a = 2.5\mathrm{AU}$ correspond to the 4:1 and 3:1 orbital resonance with Jupiter, respectively. The inclination of asteroids is concetrated among the ecliptic, but very low inclinations are rare due to gravitational interactions with the planets. Lastly, the effect of Equation 1.1 can be seen: 50% of the asteroids in the population generated by Granvik et al., 2018 has $24.6 \leq H < 25$, corresponding to a diameter of $D \leq 40\mathrm{m}$.

Among these small NEA's was the asteroid which entered Earth's atmosphere over Chelyabinsk in 2013. It is currently estimated that this asteroid had a diameter of 17 to 20 meters (Yeomans and Chodas, 2013). Assuming an albedo of $p_v = 0.14$, this would give it an absolute magnitude of $H \approx 26.5$. As previously discussed, completeness at these limiting diameters is very low. Figure 1.2 shows the completeness as a function of size according to Harris and D'Abramo, 2015. They estimate that, at their time of writing, less than 0.005% of all asteroids of this size have been identified. Through new and continued survey efforts, Stokes et al., 2017 project that the completeness at this size will increase to approximately 1.5% by 2023.

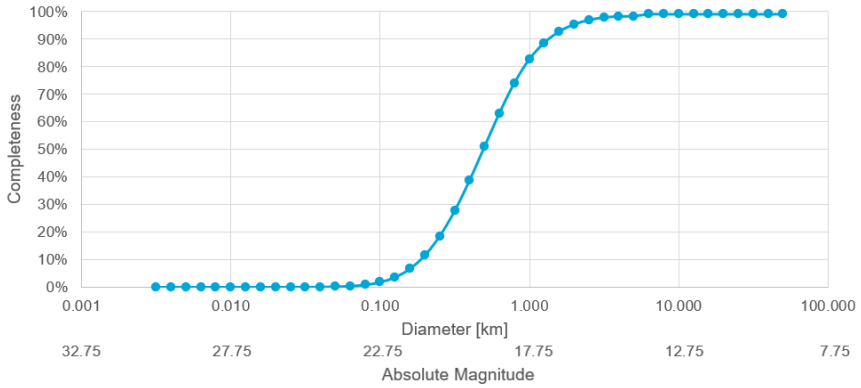

Figure 1.2: Expected survey completeness as a function of near-Earth asteroid diameter. Harris and D'Abramo, 2015

The problem can be seen in more detail in Figure 1.3. Here, Harris and D'Abramo, 2015 show the expected and identified population of NEA's as a function of their size. The effect of the continued spaceguard efforts can be seen clearly here: the asteroid population with $D > 1\mathrm{km}$ is completely known, and the population of asteroids $D > 140\mathrm{m}$ is nearing the targeted 90% completion. However, as the search efforts have been designed specifically to identify targets at this limiting size, the population with $D < 100\mathrm{m}$ is still by far and large undiscovered.

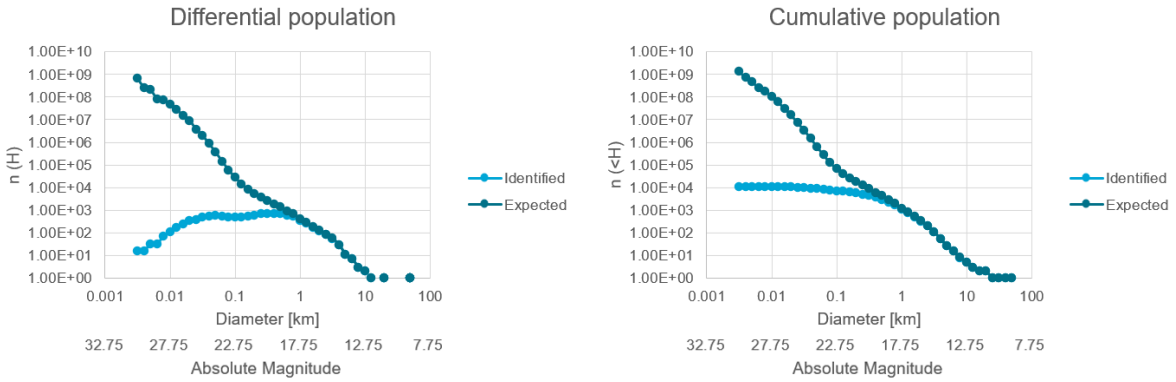

Figure 1.3: State of asteroid identification progress as of August 2014, compared to the expected number of asteroids per diameter. Note that the y-axis is logarithmic. Harris and D'Abramo, 2015

1.2. Past and Current Identification Efforts

Before continuing to the topic of the presented research, first some discourse shall be given to the missions that have resulted in the current knowledge of the NEA population. For brevity, not all missions will be listed; just a representative sample judged by the author to give a good overview of the state of the art. The missions are separated into two categories: space-based, and Earth-based. The latter comprises telescopes on Earth, with the advantage of having access to Earth infrastructure, supporting larger telescope apertures and providing practically unlimited electrical power, communication bandwidth, storage and computational resources. However, Earth-based systems are hindered by atmospheric distortion, extinction of light as it passes through the air, weather, limited search area depending on geographic position, and day-night cycles. Space-based systems contrast this: they are limited mostly by the maximum aperture of the telescopes they can support, the on-board processing capabilities and the computational power. Atmospheric and weather effects are mostly non-existant in space, however interference from the Sun, Earth and Moon should not be underestimated. To date, all NEA surveys from space have been carried out from orbits around Earth. Some proposals for deep space missions will be discussed in section 1.3.

In Figure 1.4, the contribution of several surveys to the total catalogue of NEAs is shown. The two largest contributors, the Catalina Sky Survey and the Pan-STARRS observatories, were both constructed to accomplish the goal of bringing the NEA survey completeness for asteroids $D > 140\mathrm{m}$ to over 90% of the population. The effect of these purpose-built observatories can be easily seen in their volume of discoveries. Through improvement to the facilities and processing pipelines - e.g. through better computing resources - it can be seen that the number of discoveries is still undergoing a healthy amount of growth. It is therefore important to consider the impact these surveys have on the research and proposed missions.

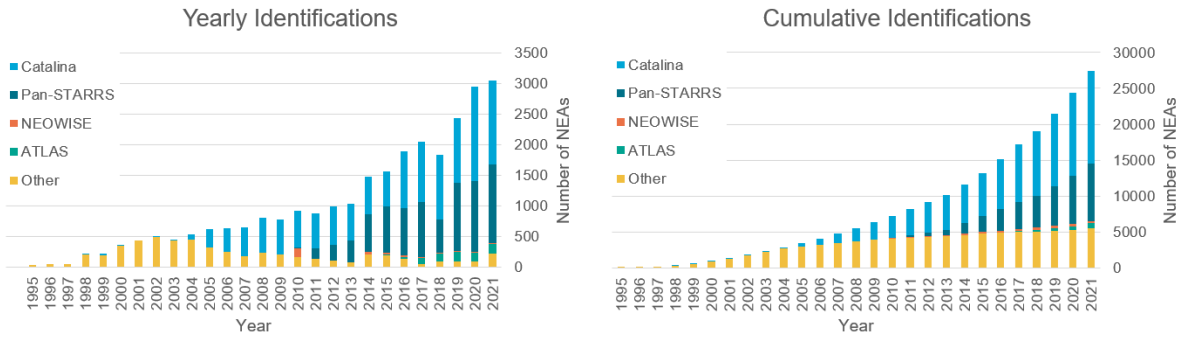

Figure 1.4: Yearly and cumulative identifications made per NEA survey from 1995 up to and including 2021. Data obtained from https://cneos.jpl.nasa.gov/stats

1.2.1. Earth-based Surveys

With almost 13000 discoveries as of the end of 2021, the Catalina Sky Survey (CSS) is currently the most succesful NEA survey by volume of detections. Operated by the University of Arizona, the CSS operates a trio of telescopes in the Santa Catalina mountains: the primary telescope is a 1.5 meter wide field reflector telescope supported by a 1.0m follow-up telescope and a further 0.7m telescope, both catadioptric. The main telescope showcases the advantages of Earth-based surveys well, as it utilizes a 111 megapixel camera with a field of view of 5 square degrees. This allows it to image the sky at a very high frequency, down to a limiting magnitude of 21.5 (Christensen et al., 2012).

The second of the major NEA surveys is the Pan-STARRS project operated by the University of Hawaii. Operating two 1.8m catadioptric telescopes, equipped with 1.4 gigapixels camera sensors, it is capable of imaging down to a visual magnitude of 24. Currently, development is underway to expand Pan-STARRS to four telescopes, and allowing it to serve as a precursor for development of the software and data processing of the Large Synoptic Survey Telescope, which will be further discussed below (Kaiser et al., 2010).

The last of the current large NEA surveys is the ATLAS (Asteroid Terrestrial-Impact Last Alert System) project. Contrary to the previously mentioned surveys, the goal of ATLAS is not to catalogue large quantities of NEAs, but to provide a last warning in case of incoming impactors. It is comprised of two 0.5m catadioptric telescopes, with plans to expand the system with three more sets of two telescopes. The survey is completely automated, and is tasked with providing impact warning for targets too small to impact until their last approach. The predicted warning times are between a day and a week (Tonry, 2010). Although this allows for alleviation of some of the damage, it is too short to take significant countermeasures such as an asteroid deflection mission or a large-scale evacuation. In addition, ATLAS suffers from the same problems as other Earth-based telescopes. For example, the 2013 Chelyabinsk meteor was not detected, as it approached Earth from the direction of the Sun.

Although not yet in operation, the expected impact of the Large Synoptic Survey Telescope (LSST) warrants a mention. Currently being constructed in the mountains of Chile, the LSST will utilize a three-mirror reflector with a 8.4m aperture, in combination with a 3.2 gigapixel sensor, making it the largest digital camera ever produced. It is expected to enter operations fully in October 2023, with a limiting magnitude of around 24.5 (Sweeney, 2006). Although the LSST is expected to complete the

goal of cataloguing 90% of the $D > 140\mathrm{m}$ NEA population in approximately 12 years, it can be seen from its limiting magnitude that detecting the faintest of NEAs will not be a succesful endeavor for an Earth-based survey, even at extreme apertures and sensor sizes. Therefore, a short overview of some space-based surveys will now be provided.

1.2.2. Space-based Surveys

As shown above, meaningfully increasing the survey completeness for asteroids under the $D > 140\mathrm{m}$ threshold is best carried out by means of a survey from space. To date, no dedicated NEA survey spacecraft has been launched, however, several missions have discovered a significant number of NEAs, most prominently among those the NEOWISE mission. Initially used for the WISE mission, imaging the entire sky in near-infrared, the spacecraft was put into hibernation after the coolant for its camera sensor ran out. In 2013, it was reawakened for the NEOWISE mission, where it would use its sensors in a non-cryogenic mode to survey for NEAs. Although the number of NEAs detected by NEOWISE is small compared to the dedicated Earth-based surveys, the new objects detected by it have been small and dark: targets which are hard to impossible to image using visual telescopes from Earth (Mainzer et al., 2014). NEOWISE thereby has shown the capability of both a space-based survey and a survey using near-infrared sensors, and its findings have contributed greatly to the capabilities for modelling the NEA population (e.g. Granvik et al., 2018).

Building on the success of NEOWISE, a new spacecraft is currently being developed by NASA under the NEOCam project. Aiming for a launch in 2026, the NEOCam mission has a dedicated design for identification of NEAs. Situated at the Sun-Earth L1 point, the mission will observe the space around Earth for potentially hazardous asteroids. It is expected that NEOCam is also capable of completing the 90% survey completeness of asteroids $D > 140\mathrm{m}$, and will be capable of imaging some asteroids down to $D > 30\mathrm{m}$, although the latter is not a primary design goal (Mainzer, 2006).

1.3. Novel Proposals

As an update to the new spaceguard objective, Shapiro et al., 2010 investigated the progress and goals of NEA cataloguing efforts. Their initial verdict was that current survey efforts are insufficient to meet the new goal, and new missions will be necessary. Several of these surveys have already been dicussed above. However, next to discussing NEAs with $D > 140\mathrm{m}$, they also state that *"... objects smaller than 140 meters in diameter are also capable of causing significant damage to Earth."* and make the recommendation that *"Because recent studies of meteor airbursts have suggested that near-earth objects as small as 30 to 50 meters in diameter could be highly destructive, surveys should attempt to detect as many 30- to 50-meter objects as possible."*.

Leading among the current proposals is the work by NASA's Jet Propulsion Laboratory (Stokes et al., 2003, Stokes et al., 2017). The initial proposal centered around updating the limiting size of to-be-detected asteroids to lower limiting diameters. The authors investigate a multitude of possibilities for accomplishing the 90% completeness at $D > 140\mathrm{m}$ goal, as well as investigating the influence on smaller diameter asteroids. Their conclusion is in line with the aforementioned: the most promising option for cataloguing a multitude of NEA's is to perform a survey from deep space. Several options are considered, among which the best performing options are 0.5 meter aperture thermal infrared telescopes at Earth-Sun L1 or in Venus-trailing orbit. The authors note no significant gain in performance by sizing up the telescope. It is also noted that no full optimization for the orbit or payload is performed. However, the proposal shows a lot of potential.

Figure 1.5 shows a projection for the improvement in survey completeness as a function of NEA diameter for a hypothetical deep space survey. A few thing are of note: Firstly, it is clear that such a survey can offer a sizeable improvement in cataloguing efforts, additionally leading to completion of the spaceguard goal in several years. However, several of the aforementioned missions currently under development also have this potential. What is more interesting is that, due to the thermal infrared telescope, cooled in deep space and largely free from interference by planets, is likely to detect a large number of small NEAs, which was hinted at by the success of the NEOWISE mission. But, the main

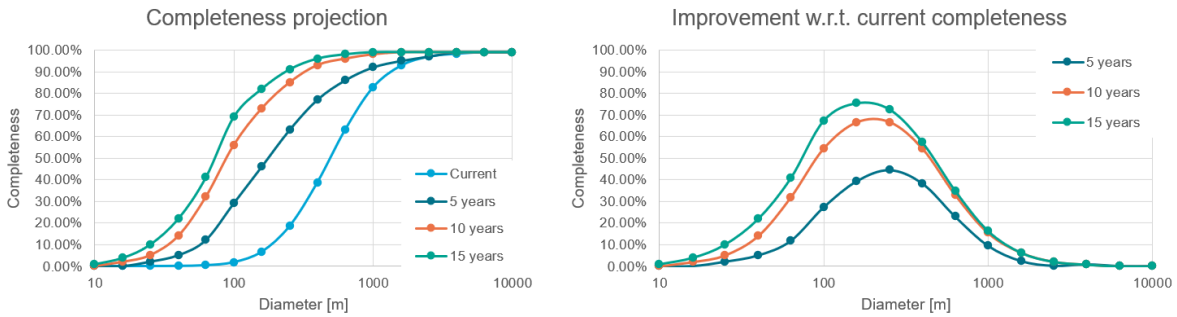

Figure 1.5: Projected improvement in survey completeness for a 5, 10 and 15 year survey from deep space. Data from Stokes et al., 2017.

bulk of the improvement is found in the $100\mathrm{m} < D < 1000\mathrm{m}$ range. Lastly, the diminishing returns of running a mission for longer become clear: as the number of undetected NEAs which fall within the limiting magnitude of the detector decreases, the performance decreases with it.

A second proposal among deep space surveys is the work of Ramirez Torralba, 2020. Her work investigates the problem of asteroid impact last warning from space. This addresses the weakness in systems such as ATLAS which was showcased by the Chelyabinsk impactor: If an asteroid approaches Earth from the Sun, it is not possible to detect it in advance from Earth, as the glare of the Sun will overpower the signal of the asteroid. Ramirez Torralba, 2020 shows that a system at the solar sail displaced Sun-Earth L1 point will provide good improvement to the effort of asteroid impact last warning strategies. However, as previously discussed, this would still leave insufficient time for e.g. a deflection mission (for the interested reader, Shapiro et al., 2010 gives a good overview of mitigation strategies). In addition, although the performance is vastly increased, performance in detecting asteroids coming from the direction of the Sun is still limited.

From the above, it is clear that current efforts are insufficient to reach the set goals for NEA cataloguing. In addition, although future surveys will reach this goal, they will only detect a small fraction of small NEAs, not cataloguing the largest population of near-Earth objects. In fact, even proposed surveys which avoid all interference from the atmosphere, the Earth and the Moon will not be capable of reaching this goal with a single spacecraft. Limitations are imposed by the location of the spacecraft, the required number of observations, and interference from Solar glare.

2

Research Outline

In chapter 1, some background on the difficulties of identification and cataloguing of NEAs was given. In this chapter, the resulting problem and associated knowledge gap will be presented. Then, the associated research questions and expected outcomes will be listed.

2.1. Problem Statement

Currently, humanity's knowledge of NEA populations is at a low level of completeness, especially for small diameter NEAs. Therefore, valuable scientific knowledge about the composition and evolution of the Solar system is unknown, and Earth is vulnerable to impacts which can be hazardous to human life and property.

It has been shown that current efforts are not adequate to reach the current goal of the spaceguard survey. Several missions have been proposed, and others are under development, which will cover this goal. However, a new more ambitious goal to identify smaller NEAs is still far out of reach. Even with a modern satellite positioned in deep space, only a limited survey completeness can be reached at limiting diameters $D < 100\mathrm{m}$. This is caused by the limitations in position of this system, the required follow-up time and the number of detections required, and interference from the Sun.

2.2. A Multi-Spacecraft Approach

To address this problem, we propose the option of a multi-spacecraft system. In recent years, spacecraft constellations have already shown a lot of potential in reaching complex mission goals. In the application of near-Earth asteroid surveys, more telescopes will firstly speed up the survey cadence, allowing the system to image the same area of sky at a faster rate. However, there are further synergystic advantages to such an approach. Three major benefits are noted in a multi-spacecraft system over a single telescope, which will be discussed in the following paragraphs.

Firstly, a multi-spacecraft system will mostly solve the problem of Solar glare: Although a spacecraft in syzygy with the Sun and an asteroid will not be able to detect the latter if it is located in the direction of the Sun, a different spacecraft located away from it might observe the Sun-asteroid arrangement from the side, allowing it to detect the target. In this way, a multi-spacecraft system is capable of minimizing the amount of blind spots in the search space. Figure 2.1 shows a visualisation of the reduction in blind areas when adding an additional spacecraft.

Secondly, using multiple spacecraft allows for easier identification and orbit determination of the NEA: Normally, a single telescope takes images in 2D of a target. As the asteroid will almost certainly be below the Rayleigh criterion of the telescope, it is not possible to estimate how close the asteroid is from its estimated diameter and the projected size on the sensor. Therefore, only the angular direction towards the target is known. Therefore, to obtain the orbit of the target requires solving Gauss' problem, which requires a minimum of three subsequent observations (six unknown parameters for the full orbit

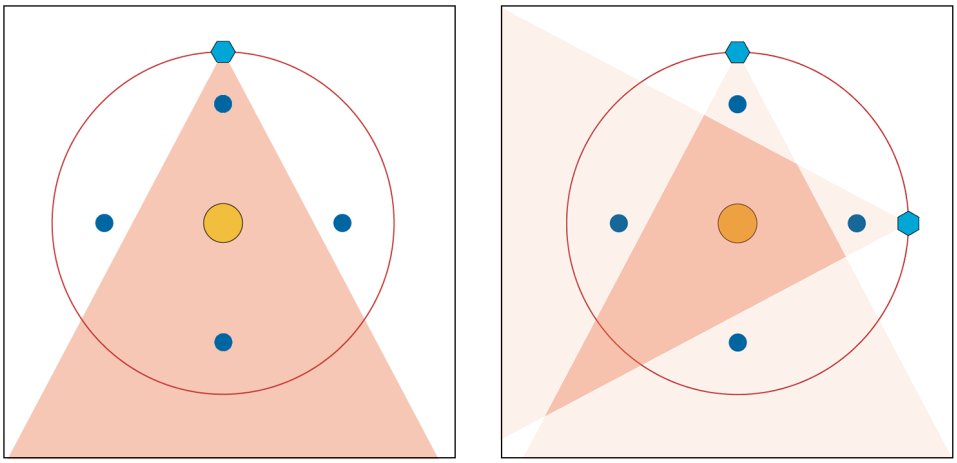

Figure 2.1: Consider a spacecraft (represented by the cyan hexagon) attempting to observe several asteroids (blue circles). Because of Solar glare and thermal limits (red-shaded area), the spacecraft is unable to observe the top and bottom NEA. However, addition of a second spacecraft greatly reduces the “blind area”: now the system can observe all four NEAs.

specification, two variables measured per observation). When using multiple spacecraft, it is possible to perform a kind of “triangulation”, provided the spacecraft and the asteroid are not colinear. This allows for solving for the three-dimensional position of the asteroid. Thus, using only two observations in time reduces the orbit determination to Lambert’s problem. This means the asteroid will only have to be within the area where telescopes can observe it for half the time as a single-spacecraft system. This is further shown in Figure 2.2, where addition of a second spacecraft allows for observing the asteroid before it moves out of the observable range.

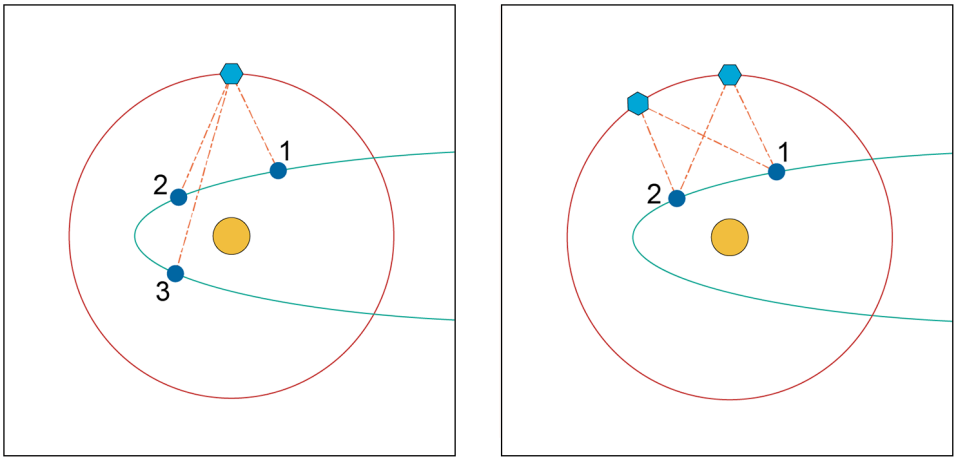

Figure 2.2: Normally, in order to perform orbit determination, the spacecraft (cyan hexagon) would have to image a target (blue cicle) three times. For targets that are hard to observe, such as a highly eccentric NEA which can only be detected close to perihelion, this leads to problems: the third detection will be hard to obtain, as the NEA moves behind the Sun into the blind area, or out of the detector’s range altogether. Addition of a second spacecraft allows triangulation, thus halving the time required to identify the asteroid, performing the necessary measurements before the asteroid moves far away again.

Lastly, a multi-spacecraft approach allows for more complex search strategies. The possibility for doing such search strategies when multiple sensors are available is demonstrated by the Cataline Sky Survey. Using their follow-up telescope, a new target is quickly selected for follow-up imaging, quickly gathering the required observations to perform orbit determination and thereby identification. In space, such a strategy would of course by more complex, as the problem becomes influenced by the location of the spacecraft. However, such an implementation will be very helpful in detecting NEAs which are only visible for a short period of time, such as highly eccentric objects with long semi-major axis, which are only visible for a short window around their perihelion. This idea is demonstrated in Figure 2.3.

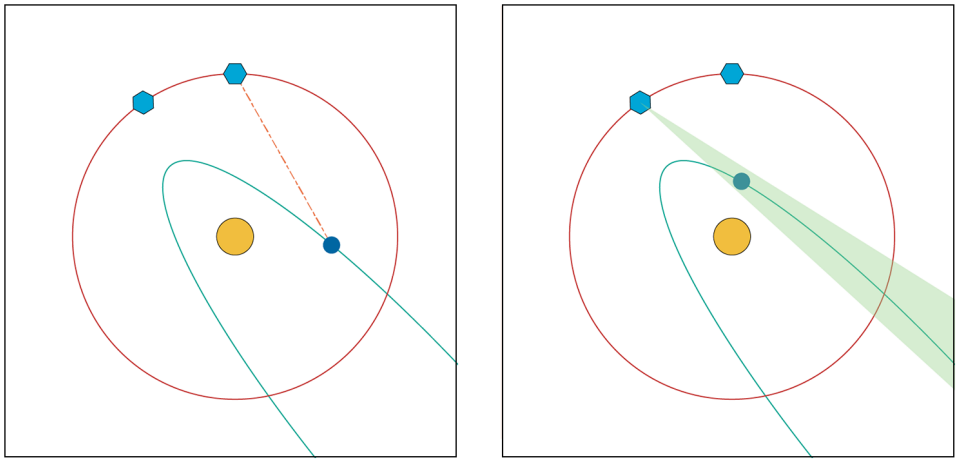

Figure 2.3: In a more advanced system, some of the spacecraft could be dedicated to follow-up observations. As soon as one spacecraft detects a target, the second spacecraft is instructed to point in the direction of the new observation. In that way, even if a target is only observable for a short period, the spacecraft will have a much larger chance of pointing towards it.

However, before such strategies can be developed and implemented in a mission, it is first required to know the location and composition of such a multi-spacecraft system. To the author's best knowledge, the behavior of a multi-spacecraft survey has never been evaluated. In addition, to adequately assess the performance, it is vital to discover where the craft in such a system should be positioned, and how they should be equipped. The aim of this work are to provide insight into these points using simulation of such a survey.

2.3. Research Questions and Expected Outcomes

To translate the aim into a concrete research topic, a main research question and a set of derived subquestions is composed. The main research question is:

What is the optimal position and composition for a system of spacecraft with the purpose of identifying and cataloguing previously unidentified near-Earth asteroids?

A few terms deserve special attention: To begin, the terms *position and composition* serve to indicate the scope of the research. As mentioned previously, no previous work has been published on multi-spacecraft NEA surveys. The current body of work on space-based surveys commonly uses general categories of orbits such as Venus-trailing orbits, or orbits at Lagrange points. In addition, either thermal infrared or a visual light telescope is used. In a multi-spacecraft system, the position should be treated in a more general sense: there is the added element of combining different positions synergistically, as explained in the previous section. Also, the composition with regards to payload is worthy of investigation: perhaps, a synergistic combination of slower but more sensitive infrared and faster but less sensitive visual light telescopes might be of merit. In addition to specifying what should be researched, these terms also limit the scope: other aspects, including - but not limited to - search strategy, communication between spacecraft, and image processing techniques will be left to further research.

The second factor of note is *identifying and cataloguing*. The distinction between observation, detection, identification and cataloguing is worth the discourse before continuing. Essentially, these terms all represent successive steps in the survey. An *observation* is when a target is within the telescope's field of view when an image is taken. Of course, this is not useful in and of itself. Therefore, a *detection* can be established when the signal-to-noise ratio of the asteroid in the image is sufficiently high. At this point, it is clear that "something" is present in the telescope's field of view. When enough detections are established within a certain time frame, it becomes possible to determine the orbit of the target,

and to see whether or not it is already known. At this point, an *identification* can be performed from the subsequent observations. Then, with the orbit of the target known, the survey can proceed to *cataloguing* the NEA by transmitting the relevant data back to Earth for analysis and storage. Thus, it is apparent that just observing or detecting an NEA is not useful in and of itself. For the information to be relevant, the system should be capable of assisting in the identification and cataloguing efforts.

The last term important to give some discourse to before further explaining the research is *unidentified* asteroids. As was discussed in section 1.2, humanity has already catalogued a sizeable portion of the NEA population. Of course, it is not neccessary to identify these targets again. Therefore, the research effort should be concentrated on solving the identified problem of improving the knowledge of the small-diameter NEA population.

In support of the main research question, in conjunction with the aim of addressing the problem through a numerical simulation, several subquestions were drafted to assist in providing an answer. The first three subquestions are related to the design of the simulation; how to accurately produce and operate a model of NEA surveys. The next three questions are related to the parameters of such missions; where the spacecraft are located and how the system is composed. Lastly, a subquestion is included which will be essential for judging the results in the context of current and future endeavors, such as those listed in section 1.2 and section 1.3. The subquestions are explained in brief below:

1. **How can the population of NEAs be accurately modelled, and how can these models be adjusted for unidentified NEA's?**: The first subquestion is related to simulation. As mentioned above, the model needs to give an accurate estimate for how the system will perform in surveying unidentified NEA's. Therefore, first a model of this population is required. Although this may seem straightforward, it might pose some challenges: after all, only the identified portion of the NEA population is known, the unidentified portion is clearly not. Fortunately, literature sources are available to assist in this process.

2. **How can surveys of NEA's by a system of spacecraft be accurately modelled?**: Having the asteroid population, the next consideration is how to model a survey of that population. Again, good sources in literature are available to assist in solving this question, although sufficient verification and validation will need to be performed.

3. **How can the position and composition of the system be optimized?**: Already mentioned above, the possibilities for positioning and composing a multi-spacecraft system grow exponentially with the number of spacecraft in the system. Therefore, a good method of optimizing the system is required. It is expected that the simulation will be computationally expensive, and possibly noisy. Therefore, selection of a proper optimization method is crucial to ensure good results.

4. **What is the effect of increasing the number of spacecraft on the process and performance of identifying and cataloguing NEA's?**: The first question related to the behavior of the system, and probably the most straightforward relation to consider when looking at the research question. Although it is apparent that an increase in the number of spacecraft will always increase the performance (or at worst, have it stay constant), the number of spacecraft is the most relevant free parameter to have results on, as it is a very important concept to explore and consider for future missions.

5. **How is the performance of possible payload compositions affected by the number of spacecraft, and what is the resulting optimal payload composition?**: Secondly, the payload of the system. As explained in section 1.3, current research often uses either a visual or a thermal infrared telescope. However, when considering a multi-spacecraft system, combinations of these are possible. It will be good to see which of the systems benefits mostly from the increase in the number of spacecraft, and whether synergistic effects occur in "hybrid" systems composed of a mix of instrumentation.

6. **How do the number of spacecraft and payload interact with the orbital parameters of the system?**: The last of the free parameters, the positioning of the spacecraft. Although it is not very crucial for the preliminary stage of mission design which is the target of this mission, it is

important to understand what the interaction between these factors is and how this affects the performance.

7. **How effective is a system of multiple spacecraft at identifying and cataloguing previously unidentified NEA's compoared to other current and future methods?**: A multi-spacecraft survey mission is a very costly endeavor, requiring several expensive spacecraft and vehicles for launching these into outer space. Although this work will not go into detail on the economics of space missions, a realistic assessment to the merits of the idea should be made to consider whether it would be worth it to develop such a mission.

It is expected that through answering this research question, several outcomes will be obtained. The main goal is to provide outcomes which are useful in doing further research into, as well as designing, future NEA survey missions. The desired outcomes of this work are thus as follows:

1. Understanding how increasing the number of spacecraft affects the performance of a NEA system. Of course, the performance will increase, however the main interest is in how much this performance increases, and thus whether such a solution is worth considering for future missions. It is expected that in addition to this, insight will be gained into any diminishing returns for higher numbers of spacecraft, and perhaps limits beyond which adding addition spacecraft provides no tangible benefit anymore.

2. A conclusion on where to focus efforts with regards to payload. Currently, thermal infrared telescopes are considered the best choice for future NEA missions (e.g. Stokes et al., 2017, Ramirez Torralba, 2020). However, perhaps the benefits of a multi-spacecraft system are expressed stronger in a visual light system, or a hybrid system might provide a synergistic benefit.

3. Insight into changes to the optimal orbital position for the spacecraft as a function of the number of spacecraft. It is expected that these quantities will undergo some change, and mapping this out allows for relating the results to the results of other studies on where to position NEA survey spacecraft.

4. Reliable estimated for what performance to expect as a higher number of spacecraft is utilized in the system. In addition, this result is also interesting is reverse: seeing what kind of system would be necessary to obtain a desired result provides a basis for designing a mission out of such a requirement.

Through fulfilling these goals and providing the expected outcomes, a useful base for further work on these kind of NEA surveys will thus be laid.

3

Survey Modelling

Space missions are very expensive to design, build, launch and operate. Therefore, it is important that all properties and behaviors of such a mission are well known in advance. Then, an accurate assessment can be made of the merits of the mission and what results are to be expected. In addition, it allows for selecting the design which will produce the best results. In order to study these properties and determine the optimum, computer simulations are an excellent tool. They allow for cheaply and rapidly testing out a lot of possible mission parameters, and recording the relevant data for easy analysis.

Currently, no model is publicly available for modelling multi-spacecraft surveys. Therefore, a simulation will be developed. During and after development, the model is also extensively verified and validated. The process for this is described in REF??. Other research (e.g. Torralba et al., 2019, Stokes et al., 2017) has demonstrated the potential for explicitly modelling out the entire survey as it would be conducted by the actual system. In this chapter, the theoretical background for the various steps in simulating a NEA survey will be given. Implementation of the simulation will then be treated in the next chapter.

The components of the simulation consist of first generating a representative population of asteroids (described in section 3.1), then, at each timestep, calculating the background and target signal (section 3.2 and section 3.3, respectively). Knowing these signals, the signal-to-noise ratios can then be determined after estimation of some of the detector properties (section 3.4). The frequency and location of the observations is determined by the search strategy, and resulting cadence (detailed in section 3.5) and lastly through repeat observations, it can be determined whether the system is capable of identifying a target (section 3.6).

3.1. Population of Asteroids

The first component of the simulation is the asteroid population model. This population was already briefly described in section 1.1. In this section, more details on the generation of the population and the process of determining the positions of the NEA's, are given. As already mentioned in section 1.1, the most comprehensive debiased population model is the one by **PopulationGranvik**. This population model was generated by propagating an intiial population of NEA's based on several known interactions (e.g. gravitational interaction with the planets), and then comparing the resulting population to the results of the NEOWISE mission. Essentially, the problem then reduces to the question: "What initial population would result in the results that are observed in the NEOWISE mission?". Then, the initial population model can be fitted to the results of the NEOWISE mission, and an accurate population model is obtained.

Of course, this results in a full population of NEA's; whereas a population of *unidentified* NEA's is required for this work. Therefore, a correction to the population was made based on the work of

PopulationHarris. To do this, the population as given by **PopulationGranvik** was separated, based on absolute magnitude, into bins of width 0.5. Then, it was assumed that the detection of NEAs is roughly uniform over the orbital parameters. The completeness statistics of **PopulationHarris** can then be used to discard a part of the population as *identified*. For example, given 10000 asteroids in the bin width XXYYZZ, where 70% is considered identified at this time, 7000 asteroids are selected at random and discarded. Of course, the assumption of uniformity in the detection of NEA's is false: highly eccentric NEA's, NEA's that are very dark, or NEA's with a high semi-major axis are more likely to be undetected. However, no data is available on this matter, and therefore no better alternative was deemed to be available. As all simulations will be affected equally, the error is judged to be sufficiently small for practical purposes.

3.2. Background Signal

BESPREKEN BIJ IMPLEMENTATION: Hoe worden achtergrondsterren weggehaald?

Before considering the existing knowledge on modelling asteroid signals, first the background in which these targets has to be observed is discussed. In this section, the current relevant body of knowledge on modelling this background signal will be listed. The background signal will be split into two components. Firstly, the background light originating from the Sun. This manifests most dramatically in the form of direct Sunlight. However, also reflections off of interplantary dust are important. This reflection manifests in the phenomena of zodiacal light and gegenschein. The second component of the background signal, is the light from outside the Solar system. This light originates from other stars and manifests mainly as a diffuse background of starlight. In addition, a very large concentration of this starlight is found around the galactic plane.

The reason for separating the background signal into these two components is straightforward: in a reference frame fixed among the stars, the background signal from outside the Solar system is practically unchanging as the spacecraft moves around the Sun; the parallax of moving a few AU is negligible on galactic scales. In constrast, the contribution of light from our Sun is directly dependent on the position of the spacecraft with regards to the Sun. In the following sections, two primary reference frames are used: a heliocentric ecliptic reference frame (A right-handed reference frame whose principal plane is the ecliptic plane, origin at the center of the Sun, and the positive X-direction towards the vernal equinox), and a galactic reference frame (A right-handed reference frame whose principal plane is the plane of the Milky Way, origin at the center of the Sun, and positive X-direction towards the galactic core). The transformations between eclpitic longitude and latitude (l_e, b_e) and galactic longitude and latitude (l_g, b_g) are as follows:

$$b_g = \sin^{-1}(\sin b_e * \sin B_{NGP}) - \cos b_e \sin b_{NGP} \sin(l_e - l_{NGP} \tag{3.1}$$

$$\sin l'_g = \frac{\sin b_e \cos b_{NGP} + \cos b_e \sin b_{NGP} \sin(l_e - l_{NGP})}{\cos b_g} \tag{3.2}$$

$$\cos l'_g = \frac{\cos(l_e - l_{NGP}) \cos b_e}{\cos b_g} \tag{3.3}$$

$$l_g = \begin{cases} \sin^{-1}(\sin l'_g) + l_{GC}; & \cos l'_g \geq 0 \\ \pi - \sin^{-1}(\sin l'_g) + l_{GC}; & \cos l'_g < 0, \sin l'_g > 0 \\ -\pi - \sin^{-1}(\sin l'_g) + l_{GC}; & \cos l'_g < 0, \sin l'_g \leq 0 \end{cases} \tag{3.4}$$

With b_{NGP} the latitude of the North Galactic Pole, approximately equal to $29.81°$ or 0.5203rad; ascending node of the Galaxy l_{NGP}, approximately $270.02°$, 4.712rad; and longitude of the galactic core l_{GC}, approximately $6.38°$, or 0.1114rad. Finally, a transformation is required to express the ecliptic coordinates in a frame which is relative to the Sun, as the Sun-based contribution will be expressed relative to the Sun. This is however simply a subtraction of the latitude $l_e^{\odot}$ and longitude $b_e^{\odot}$ of the Sun in the ecliptic frame, from the latitude and longitude of the target in the eclpitic frame:

$$l_h = l_e - l_e^{\odot} \tag{3.5}$$

$$b_h = b_e - b_e^{\odot} \tag{3.6}$$

With the reference frames defined, the individual components can be discussed. Firstly, the contribution of the Sun will be discussed, and then the background starlight for both thermal infrared and visual light.

3.2.1. Solar contribution

Modelling of the thermal infrared background radiation as a result of the light from the Sun is described by Kelsall et al., 1998, based on observations of the COBE mission. This model focusses on a modelling of the thermal state of interplanetary dust, and the resulting thermal infrared emission observed. Thus, the signal is not comprised of light originating at the Sun - but rather on the radiation from bodies heated by that light. The authors state that the albedo of particles at the relevant wavelengths is very close to zero, and therefore scattered Sunlight need not be considered; only the emissions of the particles. Thus, the zodiacal flux $Z(l, b)$ can be expresssed as an integral over the line of sight of the sensor of the various contributions (which will be discussed in more detail below):

$$Z(l,b) = \Sigma_c \int_{\lambda_0}^{\lambda_1} \int_S n_c(X,Y,Z) E_c(\lambda) B(\lambda, T) ds d\lambda \tag{3.7}$$

With n_c being the density of the dust due to a contribution c, B is the blackbody emission given by Planck's law and E_c is a wavelength-specific emission correction factor. The temperature of the dust grains is assumed to follow a power law function of distance from the Sun R:

$$T(R) = T_0 R^{-0.467} \tag{3.8}$$

Temperature T_0 at 1 AU is set to $286\mathrm{K}$, and the emissivity modifications at the $4.9\mu\mathrm{m}$ and $12\mu\mathrm{m}$ thermal infrared wavelength are 0.997 and 0.958, respectively. Then, based on observations of the COBE mission, the authors construct a parametric model, based on three contributions. The first contribution is a "donut-shaped" dust cloud centered on the Sun, and inclined $2.03°$ with respect to the ecliptic. This is the largest contributor to the density of interplanetary dust. Two more contributions which are modelled are a set of three dust bands, inclined at $0.56°$, $1.2°$ and $0.8°$. Lastly, a circumsolar ring is modelled along the orbit of the Earth, which has a higher concentration around $10°$ behind Earth in its orbit, as dust trails the planet due to its gravity. [1] An illustration of the contours of the components is seen in Figure 3.1.

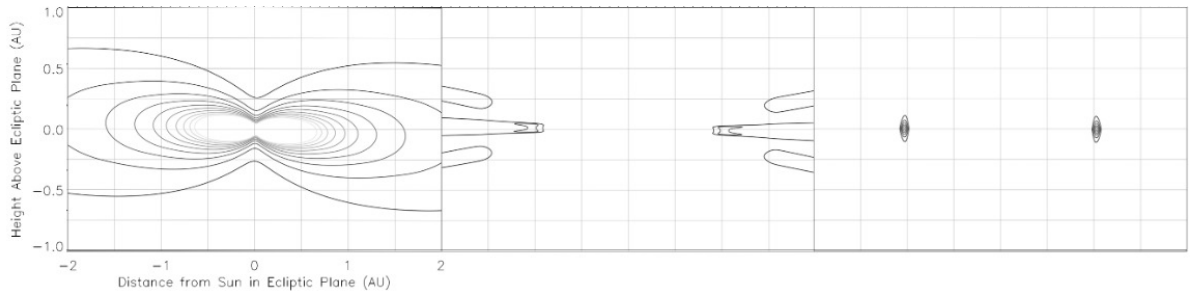

Figure 3.1: Isodensity contours of the interplanetary dust model, shown at a plane perpendicular to the ecliptic. F.l.t.r.: the dust cloud, dust bands, and the circumsolar ring. Units of the contours are $10^{-7}\mathrm{AU}^{-1}$ for the dust cloud, and $0.125 \cdot 10^{-7}\mathrm{AU}^{-1}$ for the bands and ring.

The combined density model is shown in Figure 3.2. As can be seen, the dust cloud is the largest contributor to the density of the dust cloud. With the density and temperature components known, the infrared background due to the interplanetary dust can be modelled. The only factor that needs to be added to this is the direct thermal radiation from the Sun, which can be obtained directly from Planck's law.

Combining all these components leads to the full contribution as a result of Solar radiation and interplanetary dust. An illustration of the signal can be seen in Figure 3.3. The contribution from the

[1] For conciseness, the exact model will not be described here in detail; interested readers can refer to Kelsall et al., 1998.

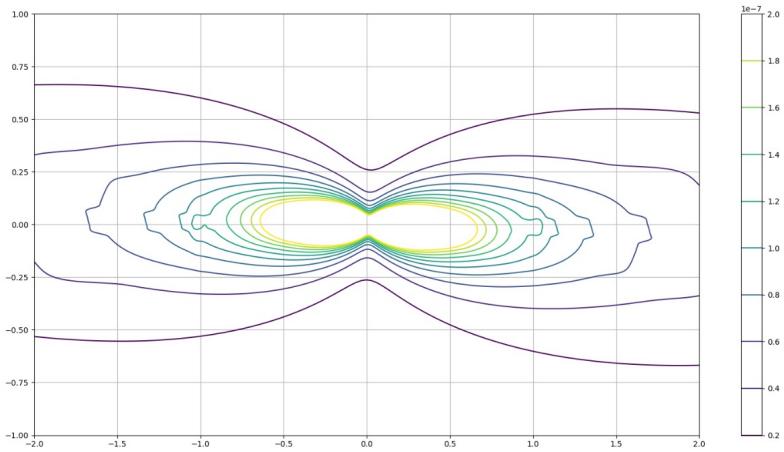

Figure 3.2: Combined isodensity contour of the interplanetary dust in a plane perpendicular to the ecliptic. TO DO: 3D PLOT

Sun, and the hot dust near the Sun, is the most important source. However, there is still a sizeable flux originating in the interplanetary dust throughout the Solar system.

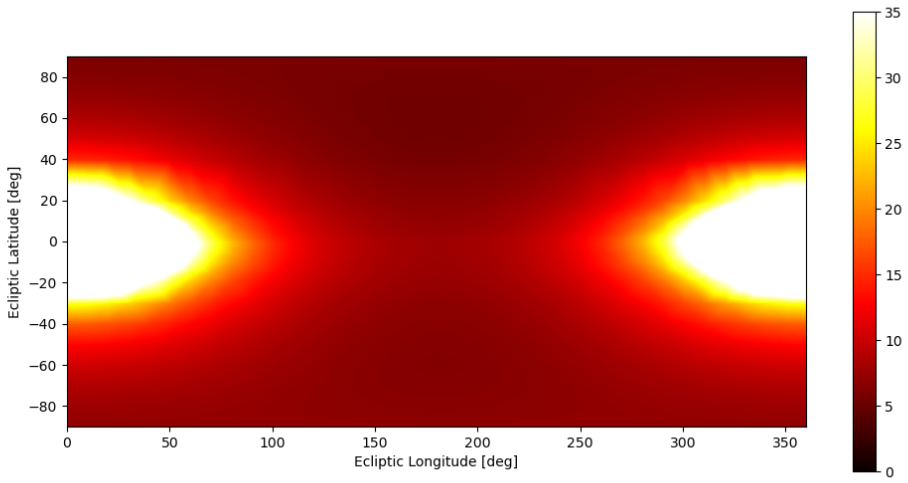

Figure 3.3: Contribution of light from the Sun to the background signal in thermal infrared, in ecliptic coordinates, as seen from a spacecraft located at (-1, 0, 0) AU. Units are Megajansky per steradian, $1\mathrm{MJy}sr^{-1} = 10^{-21}\mathrm{Wm}^{-2}\mathrm{Hz}^{-1}\mathrm{Sr}^{-1}$, and the scale is clipped at 35 $\mathrm{MJy}sr^{-1}$ for clarity.

On the other hand, the background signal in the visual spectrum is more readily available. As it can be quickly and repeatedly measured from the surface of the Earth, early measurements of this signal exist. The components of the visual light background signal are tabulated by Roach and Gordon, 1973, using data obtained from measurements. The resulting contribution from the Sun and Sunlight reflected off of interplanetary dust can be seen in Figure 3.4. Next to the obvious contribution of the Sun and zodiacal light, the phenomenon of gegenschein can be observed in the middle of the plot. Although this is the points where target asteroids are brightests, it is also a point of increased background flux. The values as tabulated by Roach and Gordon, 1973 are only valid at a distance from the Sun of $1\mathrm{AU}$. Leinert et al., 1998 offer a correction factor for changing heliocentric position of the observer as follows:

$$F(R) = F_{1\ \mathrm{AU}} R^{-2.3} \tag{3.9}$$

This correction factor accounts for both the approximate decrease in interplanetary dust density when

moving away from the Sun, as well as the decrease in solar flux. With these components, the Sun-dependent portion of the background signal is fully available for modelling.

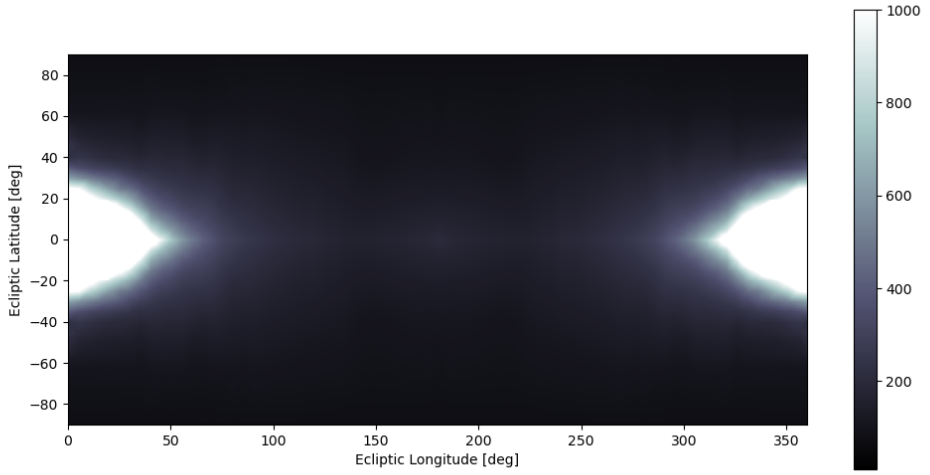

Figure 3.4: Contribution of light form the Sun to the background signal in the visual spectrum, in ecliptic coordinates, as seen from a spacecraft located at (-1, 0, 0) AU. Units are $S10_{\odot}$ or solar-type stars of 10th magnitude per square degree. $1S10_{\odot} = 9.00\mathrm{Wm}^{-2}\mathrm{Sr}^{-1}$. The scale is clipped at $1000S10_{\odot}$ for clarity.

3.2.2. Milky Way and Diffuse Starlight

For the background signal originating from the Milky Way and other diffuse starlight, similar models exist for both the thermal and infrared and the visual light spectrum. By subtraction of the signal from the Sun, zodiacal light and gegenschein, the remaining portion of the background signal could be attributed to this component. The resulting models from Kelsall et al., 1998 and Roach and Gordon, 1973 are shown in Figure 3.5 and **??**, respectively. Due to the research being more modern, and more computer and data storage resources being available at the time, the thermal infrared background model can be seen to be more detailed than the visual light spectrum model. However, other similarities, such as the light from the galactic core around $l_e = 270°$ can be observed in either. Lastly, note that while the diffuse background starlight generally has a lower magnitude than the emission and reflection of the interplantary dust, the Milky Way is brighter than the interplanetary dust in both spectra and thus warrants inclusion into the model.

A final note is to be made about individual stars: readers who occassionally take a look at the night sky are undoubtedly familiar with the fact that numerous stars outshine the diffuse background, making them appear as individual, distinct points. Naturally, these point will also appear in images taken of the sky. However, as these objects are essentially fixed with regards to the movement and timescale of human surveying efforts, they have been extensively catalogued. Therefore, removal of these points is a fairly straightforward and well-understood process (see Zackay et al., 2016 for a thorough explanation of the process), and they can be let out of the modelling effort without affecting the results.

3.3. Target Signal

TO DO: Example plots

Next to modelling the background signal, the target signal has to be modelled. Although in reality the radiation emitted or reflected by an asteroid is dependent on a lot of factors, including, but not necessarily limited to, its size, surface composition, shape, temperature and rotational motion, models exist which provide good approximations. As the asteroid population model from **PopulationGranvik**

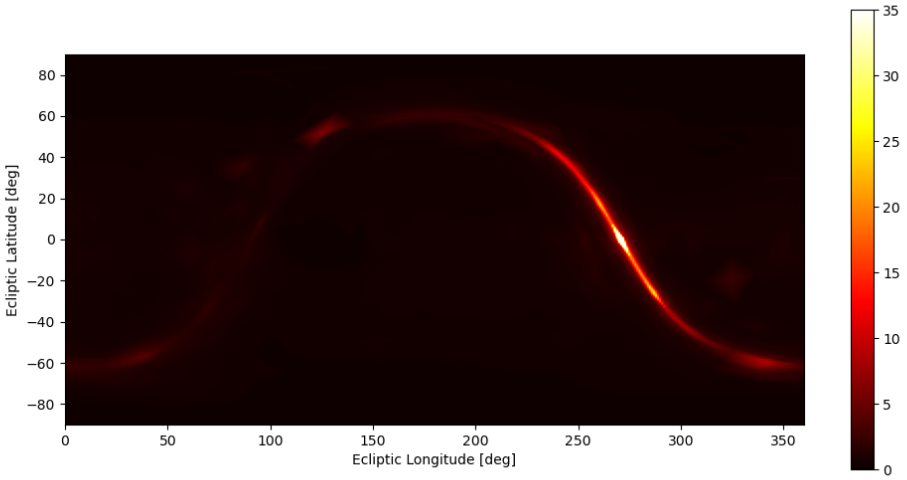

Figure 3.5: Contribution of light from the Milky Way and diffuse starlight to the background signal in thermal infrared, in ecliptic coordinates. Units are Megajansky per steradian, $1\mathrm{MJy}sr^{-1} = 10^{-21}\mathrm{Wm}^{-2}\mathrm{Hz}^{-1}\mathrm{Sr}^{-1}$, and the scale is clipped at 35 $\mathrm{MJy}sr^{-1}$ for clarity.

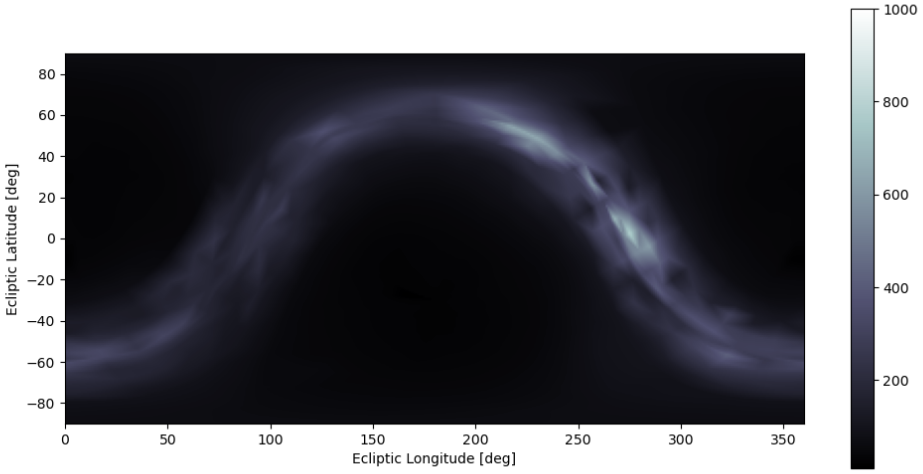

Figure 3.6: Contribution of light form the Milky Way and diffuse starlight to the background signal in the visual spectrum, in ecliptic coordinates. Units are $S10_{\odot}$ or solar-type stars of 10th magnitude per square degree. $1S10_{\odot} = 9.00\mathrm{Wm}^{-2}\mathrm{Sr}^{-1}$. The scale is clipped at $1000S10_{\odot}$ for clarity.

gives a distribution of absolute magnitudes, the starting point of these models will also be the asteroids absolute magnitude, along with the position of the asteroid and the spacecraft relative to the Sun.

Firstly, for determining the emission of an asteroid in the thermal infrared, several models have been constructed in recent years. The original model for asteroids in thermal infrared is provided in the work of Lebovsky et al., 1986. However, more recently **AsteroidNEATM** have given an updated model of the thermal emissions of asteroids, and therefore their Near-Earth Asteroid Thermal Model (NEATM) is considered the standard at time of writing.

The NEATM assumes asteroids to be spherical, nonrotating body in thermal equilibrium with the radiation emitted by the Sun. The night side of the asteroid is assumed to have a temperature of 0. The equilibrium temperature is modelled as follows:

$$T(\phi) = \begin{cases} T(0)\cos^{1/4}\phi; & \phi < 90^\circ \\ 0; & \phi \geq 90^\circ \end{cases} \tag{3.10}$$

$$T(0) = \left[(1-A)F_\odot/(\eta\epsilon\sigma)\right]^{1/4} \tag{3.11}$$

With ϕ the angular distance from the subsolar point, A the bond albedo, $F_\odot$ the incident solar flux, ϵ the emissivity, σ the Stefan-Boltzmann constant and η the so-called *beaming parameter*, a correction factor for the emission dependent on the non-sphericalness of the surface, which can be calibrated from observations. For the NEATM, this value is set to $\eta = 1.22$.

With the temperature distribution known, the emission can be determined through integration of Planck's law over the visible hemisphere. For this, the size of the asteroid needs to be determined, which can be done using Equation 1.2. Of course, this calculation is sensitive to the assumed value of the albedo. Estimation of this albedo using current data is difficult, however a system utilizing both visual and thermal infrared measurements can use this dependancy on albedo to calculate the asteroid's size *and* albedo, instead of only the absolute magnitude.

Calculation of target signal in the visual spectrum is more straightforward, as no integration is needed; a simple phase equation is readily available to obtain the apparent visual magnitude V, as detailed by Stokes et al., 2003:

$$V = H + 5\log r\Delta - 2.5\log\left[(0.85)\Phi_1 + 0.15\Phi_2\right] \tag{3.12}$$

$$\Phi_1 = e^{-3.33\left(\tan\frac{\alpha}{2}\right)^{0.63}} \tag{3.13}$$

$$\Phi_2 = e^{-1.87\left(\tan\frac{\alpha}{2}\right)^{1.22}} \tag{3.14}$$

For solar elongations less than 60 degrees, Stokes et al., 2003 suggest using a modified equation instead:

$$V = H + 5\log r\Delta + 5.03 - 10.373\log(\pi - \alpha) \tag{3.15}$$

In these equations, H is the absolute magnitude, α is the solar phase angle, r is the distance from the Sun to the target and Δ is the distance from the observer to the target. From the definition of apparent magnitude it follows that:

$$\frac{F_2}{F_1} = 100^{\frac{\Delta V}{5}} \tag{3.16}$$

As the Sun has an apparent magnitude of $V_\odot = -26.74$, and a flux of $F_\odot = 1361\mathrm{Wm}^{-2}$, the visual flux can be calculated by:

$$F_t = F_\odot 100^{\frac{-26.74-V_t}{5}} \tag{3.17}$$

It is here where part of the difficulty of detecting very small NEA's becomes apparent: relative to a $D = 3.5\mathrm{km}$ asteroid ($V \approx 15$), a $D = 350\mathrm{m}$ asteroid ($V \approx 20$) only results in 1/100th of the flux, and a $D = 35\mathrm{m}$ asteroid ($V \approx 25$) will only give off 1/10,000th of the flux in both spectra. Note also that there is no *inherent* advantage to either method in detecting small NEA's when considering the target signal. However, the thermal infrared background signal is relatively lower relative to the target signal (Stokes et al., 2003).

3.4. Hardware Properties and Signal-to-Noise Ratio

In addition to the signal properties, the hardware used to image the target is also of interest. Some of the properties of the hardware can then be used to compute the signal-to-noise ration (SNR) of the target, and some other properties will be used in the next section to determine the search strategy and cadence. Stokes et al., 2017 gives a description of representative hardware for current and upcoming space survey telescopes. The overview can be seen in Table 3.1. For the thermal infrared, a HgCdTe detector is utilized, for the visual light a silicon CCD.

Table 3.1: Representative hardware properties for space-based survey telescopes. (Stokes et al., 2017)

Parameter	**Thermal Infrared**	**Visual Light**
Aperture [m]	0.5	0.5
Field of view [deg]	1.7 x 7.13	10.6 x 5.3
Bandpass [μm]	6 - 10	0.4 - 1.0
Integration time [s]	150	24
Quantum efficiency [%]	65	88
Dark current [e-/s]	1	0.00055
Read noise [e-]	22	4

Two important observations should be made from the data in Table 3.1. Firstly, the visual light system has better specifications with regards to noise and quantum efficiency. This is due to the more advanced level of technology in CCD development compared to thermal infrared detectors. Secondly, the square angle subtended by the visual light sensor is almost five times as large as the thermal infrared sensor, and the required integration time is less than one sixth. The former factor is also due to discrepancies in technological development, the latter is a result of the weaker signal in the thermal infrared band. Together, these factors result in a sizeable decrease in survey cadence, which will be discussed in the next section. A last factor which is not shown in the table is the requirement for thermal infrared telescopes to be cooled to very low temperatures, to avoid the heat of the telescope itself interfering with the measurements. Visual light telescopes are not hindered much by their own temperature, as spacecraft at normal operating temperatures emit very little visible light.

The signal-to-noise ratio of the observation can then be calculated by dividing the signal in e^- by the root-sum-square of the noise terms, assuming the noise terms to be independent (Adams et al., 2018):

$$SNR = \frac{S_t}{\sqrt{S_t + S_b + D + R^2}} \tag{3.18}$$

The target signal S_t and background signal S_b can be calculated from the flux F as follows:

$$S_t = \frac{1}{hc} A \tau k_f Q_e F_t \tag{3.19}$$

$$S_b = \frac{1}{hc} A \tau Q_e F_b \tag{3.20}$$

Here, A is the telescope aperture, τ the integration time of the image, k_f is the *straddle factor*, a correction factor for the diffraction of a point source ($k_f \approx 0.9$), Q_e the quantum efficiency, and h and c the Planck constant and speed of light, respectively. The noise terms in the SNR equation are:

- $\sqrt{S_t}$: the poisson noise of the target signal.
- $\sqrt{S_b}$: the poisson noise of the background signal. Note that the background signal itself can be subtracted fairly easy, and thus only the poisson term has to be considered (see Zackay et al., 2016).
- $\sqrt{D}$: the poisson term of the dark current noise. The mean dark current can be removed through proper sensor calibration (see Owen, Jr., 2013).
- $\sqrt{R}$: the readout noise.

Thus, the SNR of every target can be calculated at any point in time from any telescope in space in both the thermal infrared and visual light spectrum.

3.5. Search Strategy and Cadence

Next, it is important to consider how the telescope will conduct the survey. Of course, a telescope can not view in all directions simultaneously. Very little literature exists on setup and optimization of such search strategies. Grav et al., 2019 provides some guidance based on the search strategy for the NEOCam mission. Essentially, the telescope performs a grid-like search, from north to south and west to east. Each section of the sky is revisited four times in a short time to allows for determining the direction of motion of targets, which aids in the precision of orbital determination. Therefore, the survey cadence (the period of imaging the entire sky; i.e. a survey cadence of ten implies the telescope images the entire sky in ten days) can be approximated from the field-of-view and integration time, assuming a slew rate of $0.5\mathrm{degs}^{-1}$ and a settle time of $10\mathrm{s}$ as follows for the visual light telescope:

$$T_{survey} = 4\frac{41253\mathrm{deg}^2}{10.6 * 5.3} * (24 + 10.6/0.5 + 10) = 162134\mathrm{s} \approx 1.88\mathrm{days} \tag{3.21}$$

Which, at a duty cycle of just over 90% represents a fair assumption of the visual survey cadence of 2 days. Similarly, a survey cadence of 21 days was calculated for the thermal infrared system. Note that, as already alluded to in the previous section, the thermal infrared system has a far lower survey cadence, which will hinder the identification performance. Therefore, no system can yet be said to be superior: the thermal infrared system benefits from increased imaging performance, but a worse survey cadence.

3.6. Detection and Identification

From the signal-to-noise ratio, detection and identification can finally be established. Firstly, detection of the signal from the noise. As described by Stokes et al., 2017, detection in processed images is a probabilistic process. At low SNR (SNR < 1), while detection is possible, the detection should be rejected because the probability of false detections becomes too high. Conversely, at high SNR (SNR > 5), detection becomes almost certain. Modelling the process by a normal distribution allows for the intermittent range of SNR to be approximated by an integrated Gaussian. This distribution can be seen in Figure 3.7.

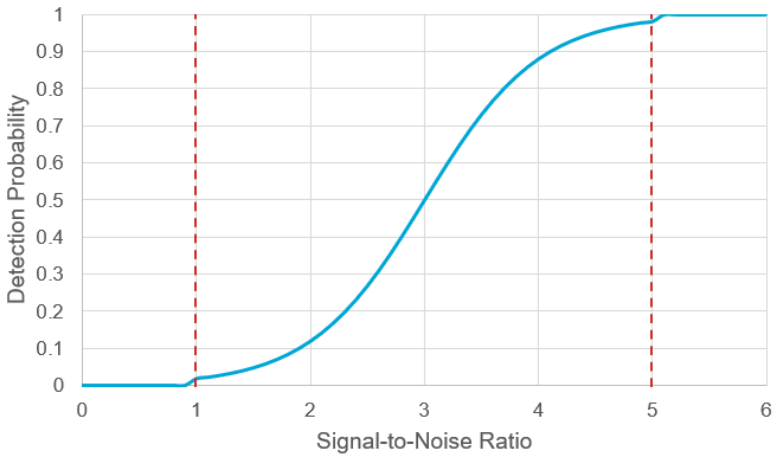

Figure 3.7: Detection probability as a function of signal-to-noise ratio according to an integrated Gaussian. The function is truncated to 0 at SNR < 1, and to 1 at SNR > 5

The process of identification is slightly more complicated. In essence, the process of solving for the orbit of a target asteroid using a single telescope uses Gauss' method, to obtain an orbit from three sets of angular measurements and the time between these. When multiple spacecraft are used and

trangulation can be performed, two sets of positions and the time between these is enough to solve for the orbit, per Lambert's problem (see e.g. Curtis, 2005 for a thorough treatment of both methods). Theoretically, the time between these observations does not matter much, as long as the period is long enough to ensure that the curvature of the arc is larger than the uncertainty in the measurement (Owen, Jr., 2013). However in practice, the problem of *linking* the observations arises: how does the system know that two observations spaced far apart in time belong to the same object? Currently, in practice, this results in a maximum time of between 30 and 90 days (Adams et al., 2018, Stokes et al., 2017). However, it is expected that the resulting maximum will be more towards the maximum due to new techniques such as those presented by Milani et al., 2004 and subsequent papers.

However, these methods rely on data being available throughout the system. It is currently unclear what data would need to be shared precisely, as no multi-spacecraft surveying systems have been researched to that level of detail to date. However, as e.g. Stokes et al., 2017 state, communication of survey results will be a point of attention for all deep-space surveying missions, not just multi-spacecraft ones, and an advanced communication system along with on-board data processing will be required. Luckily, modern techniques such as machine learning are being used to find computationally unintensive and simple solutions to the image processing pipeline (see e.g. Sedaghat and Mahabal, 2018). Therefore, this point will be considered to be out of scope of the research presented in this report.

With the detection and identification treated, a full overview has thus been presented of the process from obtaining the signal of both background and target, calculating the resulting SNR, and establishing detection and identification of NEA's. In the next chapter, implementation of these methods will be discussed.

4

Experimental Methodology

4.1. Simulation Overview

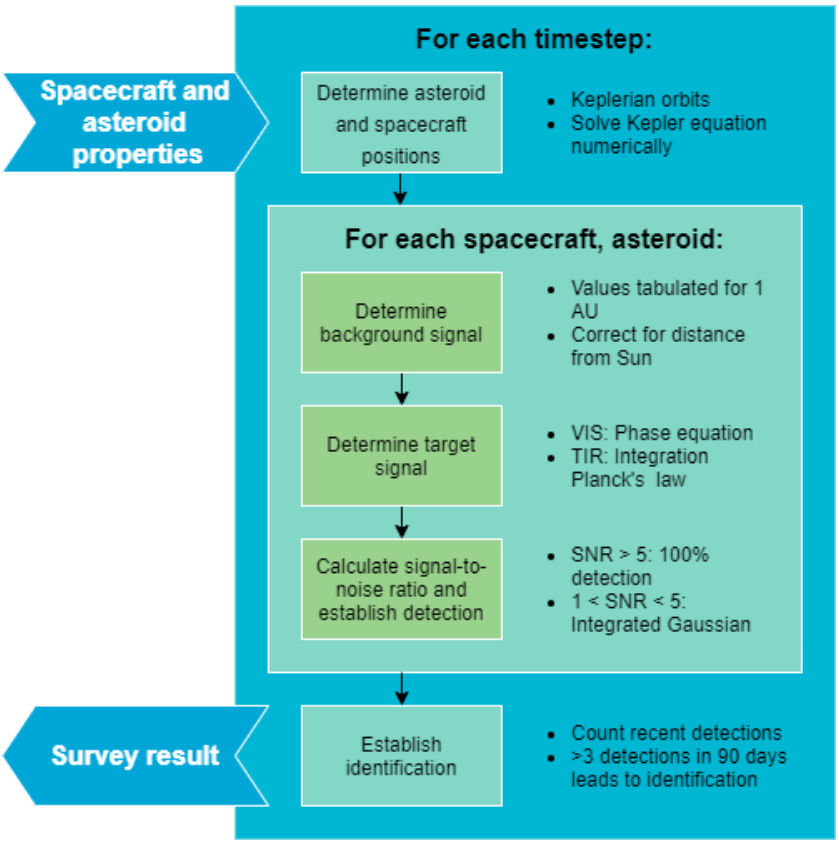

Figure 4.1: Overview of the simulation architecture and main loops.

The architecture of the simulation is shown in Figure 4.1. On the top left, the main input parameters to the model are displayed. These are primarily the spacecraft and asteroid properties. Both of these consist of a full set of Keplerian orbital elements per spacecraft or asteroid. The asteroid properties furthermore include the albedo, size, and absolute magnitude of each asteroid; the spacecraft properties include which type of payload the spacecraft is carrying.

The simulation consists of a nested loop. Firstly, at the start of each timestep (the time between the timesteps is determined by the survey cadence), the positions of all asteroids and spacecraft are determined by propagation of their orbital elements. Then, in the inside loop, each spacecraft is checked

against each asteroid to see if it can detect said asteroid. This is done through calculation of the signal-to-noise ratio (SNR). Lastly, as it is known which asteroids got succesfully detected by which spacecraft, it can be determined if asteroids have been identified. Then, at the end of the simulation, the result is a list of the asteroid population in addition to whether they have been detected, and if so, when. Of course, this data can be further processed.

4.2. Implementation
4.3. Optimization Methods
4.4. Experimental Process

5

Results

5.1. Number of Spacecraft
5.2. Payload
5.3. Orbital Elements I: Co-orbital Spacecraft
5.4. Orbital Elements II: Non Co-orbital Spacecraft
5.5. Explanation of Observed Phenomena
5.6. Predicted Performance and Implications for Missions Design

6

Sensitivity Analysis

6.1. Expected Performance
6.2. Optimization Results
6.3. Hardware and Survey Properties

7

Conclusion

7.1. Opportunities for Mission Design
7.2. Recommendations for Further Research

A

Verification and Validation

Bibliography

Adams, E. et al. (2018). *Analysis of alternatives for near earth object detection, tracking and characterization.* (tech. rep.). John Hopkins Applied Physics Laboratory.

Bowell, E. et al. (1989). Application of photometric models to asteroids. *Asteroids II*.

Chiarenza, A. A. et al. (2020). Asteroid impact, not volcanism, caused the end-cretaceous dinosaur extinction. *Proceedings of the National Academy of Sciences USA*, *117*.

Christensen, E. et al. (2012). The catalina sky survey: Current and future work. *Not published*.

Curtis, H. (2005). *Orbital mechanics for engineerings students*. Elsevier.

Granvik, M. et al. (2018). Debiased orbit and absolute-magnitude distributions for near-earth objects. *Icarus*, *312*.

Grav, T. et al. (2019). Neocam survey cadence and simulation. *50th Lunar and Planetary Science Conference*.

Harris, A. (2008). What spaceguard did. *Nature*, *453*.

Harris, A., & D'Abramo, G. (2015). The population of near-earth asteroids. *Icarus*, *257*.

Ivanov, B. (2008). Size-frequency distribution of asteroids and impact craters: Estimates of impact rate. *Catastrophic events caused by cosmic objects*.

Kaiser, N. et al. (2010). The pan-starrs wide-field optical/nir imaging survey. *Ground-based and Airborne Telescopes*, *7733*.

Kelsall, T. et al. (1998). The cobe diffuse infrared background experiment search for the infrared background. ii. model of the interplanetary dust cloud. *The Astrophysics Journal*, *508*.

Lebovsky, L. A. et al. (1986). A refined "standard" thermal model for asteroids based on observations of 1 ceres and 2 pallas. *Icarus*, *68*.

Leinert, C. et al. (1998). The 1997 reference of diffuse night sky brightness. *Astronomy and Astrophysics Supplement Series*, *127*.

Mainzer, A. (2006). Neocam: The near-earth object camera. *Bulletin of the American Astronomical Society*, *38*.

Mainzer, A. et al. (2014). Initial performance of the neowise reactivation mission. *The Astrophysics Journal*, *792*.

Milani, A. et al. (2004). Orbit determination using very short arcs: I. admissible regions. *Celestial Mechanics and Dynamical Astronomy*, *90*.

Morrison, D. (1992). *The spaceguard survey* (tech. rep.). NASA.

Owen, Jr., W. (2013). *Methods of optical navigation* (tech. rep.). NASA.

Ramirez Torralba, O. (2020). *Mission analysis of space-based telescopes to detect impacting near-earth objects* (Master's thesis). TU Delft. The Netherlands.

Roach, F. E., & Gordon, J. L. (1973). The light of the night sky. *Geophysics and Astrophysics Monographs*.

Sedaghat, N., & Mahabal, A. (2018). Effective image differencing with convolutional neural networks for real-time transient hunting. *Monthly notives of royal astronomy society*, *476*.

Shapiro, I. I. et al. (2010). *Defending planet earth: Near-earth object surveys and hazard mitigation strategies* (tech. rep.). Space Studies Board, National Research Council.

Stokes, G. H. et al. (2003). *Study to determine the feasbility of extending the search for near-earth objects to smaller limiting diameters* (tech. rep.). NASA Science Mission Directorate.

Stokes, G. H. et al. (2017). *Update to determine the feasibility of enhancing the search and characterization of neos* (tech. rep.). NASA Science Mission Directorate.

Sweeney, D. (2006). Overview of the large synoptic survey telescope project. *Ground-based and Airborne Telescopes*, *6267*.

Tonry, J. (2010). An early warning system for asteroid impact. *Publications of the Astronomical Society of the Pacific*, *123*.

Torralba, O. R. et al. (2019). Simulation of sky surveys with the flyeye telescope. *1st NEO and Debris Detection Conference*.

Yeomans, D., & Chodas, P. (2013). Additional details on the large fireball event over russia on feb 15, 2013 [Retrieved from archive: https://web.archive.org/web/20130430164941/http://neo.jpl.nasa.gov/news/fireball_130301.html].

Zackay, B., Ofek, E., & Gal-Yam, A. (2016). Proper image subtraction - optimal transient detection, photometry and hypothesis testing. *The Astrophysics Journal*, *830*.